RSC Advances

ROYAL SOCIETY OF CHEMISTRY

www.rsc.org/advances

One-pot Synthesis of Hierarchical Mesoporous SnO_2 Spheres Using Graft Copolymer: Enhanced Photovoltaic and Photocatalytic Performance

Jung Tae Park,[a,b] Chang Soo Lee,[a] Jong Hak Kim[a,*]

[a] *Department of Chemical and Biomolecular Engineering, Yonsei University, 262 Seongsanno, Seodaemun-gu, Seoul 120-749, South Korea*

[b] *Department of Chemical Engineering, Massachusetts Institute of Technology, 77 Massachusetts Ave., 66-325, Cambridge, MA, 02139, USA*

[*] To whom correspondence should be addressed

Tel: +82-2-2123-5757, Fax: +82-2-312-6401

E-mail: jonghak@yonsei.ac.kr

Table of content

Hierarchical mesoporous SnO_2 spheres with a large surface area were synthesized via a facile solvothermal reaction using graft copolymer template.

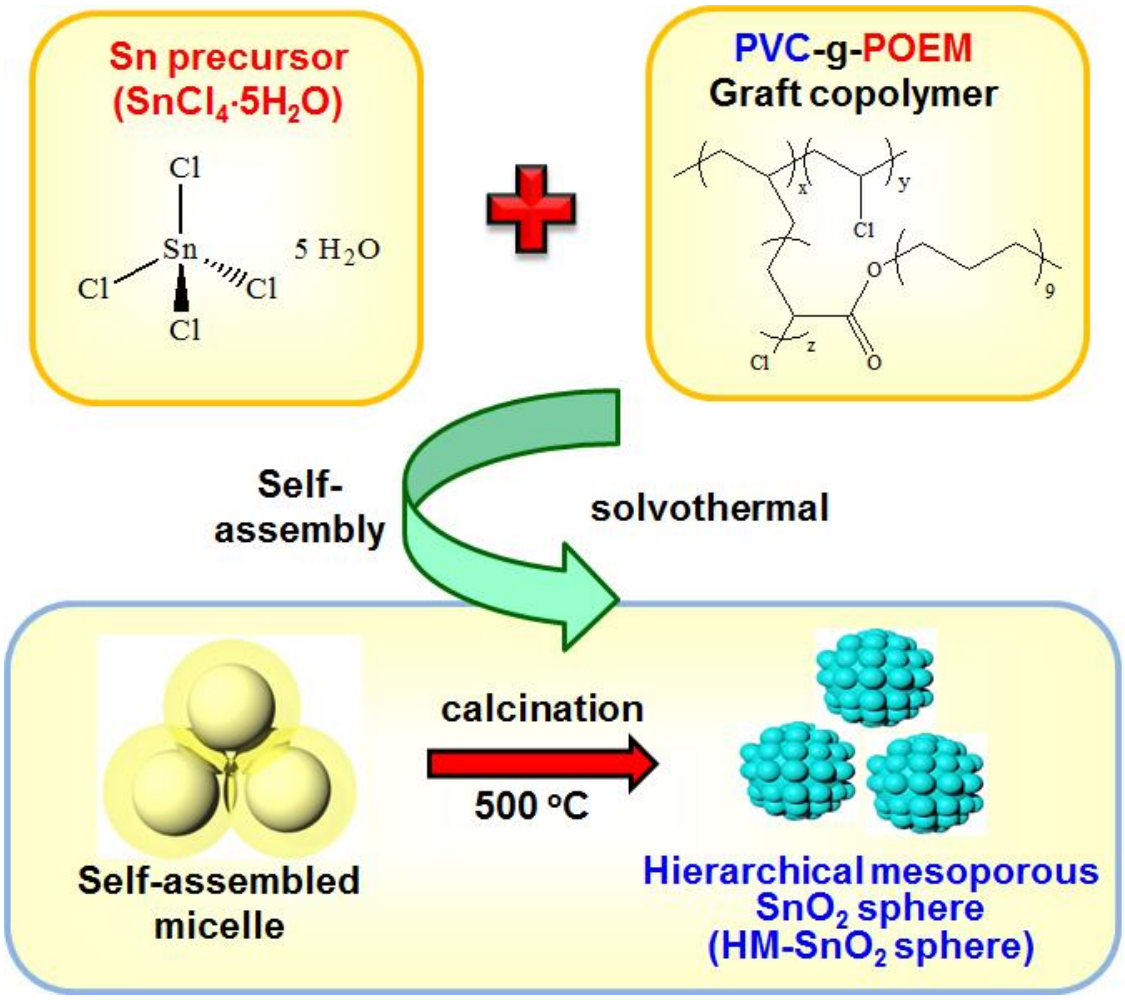

Abstract

We synthesized hierarchical mesoporous SnO_2 (HM-SnO_2) spheres with a large surface area (85.3 m^2 g^{-1}) via a one-pot controlled solvothermal process using tin chloride pentahydrate and graft copolymer, i.e., poly(vinyl chloride)-*g*-poly(oxyethylene methacrylate) (PVC-*g*-POEM) as a Sn precursor and structure directing agent, respectively. Solid-state dye-sensitized solar cells (ssDSSCs) fabricated with HM-SnO_2 spheres on an organized mesoporous SnO_2 interfacial (om-SnO_2 IF) layer as the photoanode had a long-term stable efficiency of 3.4% at 100 mW/cm^2, which was much higher than that of ssDSSCs with a photoanode comprising nonporous SnO_2 (NP-SnO_2) spheres (1.9%). We attributed the enhanced device performance of ssDSSCs fabricated with HM-SnO_2 photoanode to the well-organized hierarchical structure with dual pores (23.5 and 162.3 nm), which provided a larger surface area, improved light scattering, and decreased charge recombination than nonporous SnO_2 (NP-SnO_2) photoanode. We confirmed this by reflectance, incident photon to current conversion efficiency (IPCE), and intensity modulated photocurrent/voltage spectroscopy (IMPS/IMVS) measurements. Introduction of an om-SnO_2 IF layer between the HM-SnO_2 spheres and fluorine-doped tin oxide (FTO) substrate enhanced light harvesting, increased electron transport, reduced charge recombination, and decreased interfacial/internal resistance. Photocatalytic tests indicated that HM-SnO_2 spheres showed high activity with good recyclability for photodegradation of methyl orange under UV light irradiation.

Keywords: dye-sensitized solar cell (DSSC); photocatalyst; tin oxide (SnO_2); hierarchical mesoporous structure; graft copolymer.

Introduction

Dye-sensitized solar cells (DSSCs) have attracted considerable research interest since the seminal study in 1991 by Gratzel and co-workers, [1] because DSSCs have high efficiency, are low cost, easy to fabricate, have low manufacturing toxicity, are amenable to scale-up, and cell design is flexible. Several approaches have been developed to synthesize the individual components of DSSCs such as the photoanode,[2-4] sensitizer,[5,6] counter-electrode,[7,8] and electrolyte.[9,10] To date, the highest light-to-electric conversion efficiency of 15% was achieved by optimizing the semiconductor photoanode with an organic-inorganic hybrid perovskite absorber.[11] For the most part, TiO_2 semiconductors have been the metal oxide photoanode of choice for DSSCs due to their superior device efficiency resulting from their high specific surface area and relevant band gap position (3.0 eV).[12]

However, the wide band gap semiconductor SnO_2 (3.6 eV) has attracted much scientific attention due to its high electronic conductivity/mobility and good stability under long-term UV irradiation, which make it suitable as a photoanode material for DSSCs.[13] Li and co-workers prepared branch-type SnO_2 nanowires with efficient electron channels and excellent light scattering properties, and obtained a photovoltaic efficiency of 4.23% after $TiCl_4$ post-treatment.[14] Recently, Ramakrishna and co-workers developed SnO_2 flower-shaped nanostructures using an electrospinning method and reported a photovoltaic efficiency of 3.0%, which was much higher than that reported for a SnO_2 fiber system.[15] Tremel and co-workers reported that the use of SnO_2 nanostructures prepared *via* a microwave-assisted solvothermal process enhanced DSSC efficiency up to 3.16%.[16] In addition, Toupance and co-workers reported an efficiency of 3.2 % of a DSSC using tin dioxide nanoparticles of different sizes and shapes as a photoanode.[17] However, there are only a few reports of solid-state DSSCs (ssDSSCs) with SnO_2 nanostructures as a photoanode, presumably because of

difficulties in generating large pores, which are important for pore filling by solid polymer electrolyte.[18,19]

In recent years, a great deal of research has focused on using semiconductor metal oxides as photocatalysts due to their potential applications in environmental remediation. A photocatalyst should have high photocatalytic activity with low toxicity and excellent photocatalytic stability. Like many semiconductor metal oxides, use of nanoscale SnO_2 structures can potentially increase photocatalytic performance because these structures have a high specific surface area that facilitates efficient degradation of environmental pollutants, in addition to excellent stability as well as acid and alkali resistant properties. Xiong and coworkers reported that the photocatalytic activity of SnO_2@CdS nanowire heterostructures increased by more than 109% relative to that of neat SnO_2 nanowires.[20] Furthermore, Zhu and co-workers suggested that the photocatalytic activities of α-Fe_2O_3@SnO_2 core-shell shuttle-like nanocomposites were strongly dependent on the presence of core-shell heteronanostructures.[21] SnO_2, however, has only been used as a minor component of semiconductor composite photocatalysts. Hierarchical mesoporous nanostructures consisting of small particles and aggregated nanostructures can also potentially be used in photocatalytic devices. Small particles would provide a large surface area for photodegradation reactions, whereas a secondary aggregated nanostructure could potentially reflect incident photons to prolong their traveling distance, thereby improving light harvesting. A facile method to prepare hierarchical mesoporous SnO_2 nanostructures with the desired characteristics is therefore critical if these nanostructures are to be used for practical photocatalytic applications.

One approach that can be taken to improve DSSC performance is to control the interface between the fluorine-doped tin oxide (FTO) substrate and the main semiconductor

photoanode layer. Recently, Kim and co-workers demonstrated that the presence of a multi-functional, organized mesoporous SnO_2 interfacial (om-SnO_2 IF) layer improved light harvesting, enhanced electron transport, reduced recombination, and decreased interfacial/internal resistance compared to when this layer was not present.[22] Lee and coworkers reported improved DSSC performance based on the presence of a nanoparticle-based ultrathin SnO_2 layer as a buffer layer prepared using a layer-by-layer self-assembly technique.[23] Solid electrolytes can also enhance the stability and photovoltaic performance of DSSCs. However, ssDSSCs fabricated with solid electrolyte typically perform less well than their liquid electrolyte counterparts. This is mostly due to insufficient penetration of the large molecular volume solid electrolyte into the less-organized particulate photoanode, resulting in increased electrode/electrolyte interfacial resistance.[24] Hierarchical mesoporous nanostructures are promising ssDSSC photoanode candidates due to their inherently high porosity, ordered large pores, and good interconnectivity.

Mesoporous SnO_2 nanostructures hundreds of nanometers in size that show monodispersity are of particular interest, because these nanostructures can simultaneously increase surface area, porosity, and adsorption, and have been shown to enhance the performance of gas sensors and lithium storage devices.[25-27] Mesoporous SnO_2 nanostructures are generally prepared using a hydrophilic homopolymer such as poly(vinyl pyrrolidone) or poly(ethylene glycol). However, a homopolymer functions as a compatibilizer in hydrothermal processes, rather than a structure-directing agent. Amphiphilic nanostructural copolymers such as block and graft copolymers are better candidates than hydrophilic homopolymers because Sn precursors would be selectively incorporated into hydrophilic domains during the hydrothermal reaction, resulting in formation of a hierarchical mesoporous structure. Although titania (TiO_2) with a hierarchical mesoporous structure has

been suggested for DSSC applications,[18,19] hierarchical mesoporous SnO_2 nanostructures with two pore sizes and large pores have not previously been reported.

In this work, thus, we synthesized hierarchical mesoporous SnO_2 (HM-SnO_2) spheres for photovoltaic and photocatalytic applications via a facile solvothermal reaction using graft copolymer as a structure-directing agent. Graft copolymer of poly(vinyl chloride)-*g*-poly(oxyethylene methacrylate) (PVC-*g*-POEM) was synthesized via atom transfer radical polymerization (ATRP). Graft copolymers are easier to synthesize and cost less than block copolymers. HM-SnO_2 spheres were characterized by Field emission-scanning electron microscopy (FE-SEM), energy-filtered transmission electron microscopy (EF-TEM), X-ray diffraction (XRD), in addition to Brunauer-Emmett-Teller (BET) and Barrett–Joyner–Halenda (BJH) measurements. An om-SnO_2 IF layer was utilized as a buffer layer in ssDSSCs with a solid electrolyte, and the influence of the material structure on photovoltaic performance was also investigated. Photovoltaic and photocatalytic cells based on HM-SnO_2 spheres were fabricated and characterized in detail by measuring reflectance and incident photon to current conversion efficiency (IPCE), by generating photocurrent density-voltage (J-V) curves, and by performing intensity-modulated photocurrent/voltage spectroscopy (IMPS/IMVS).

Experiment Section

Materials

Poly(vinyl chloride) (PVC, M_w = 97,000 $gmol^{-1}$, M_n = 55,000 $gmol^{-1}$), poly(oxyethylene methacrylate) (POEM, poly(ethylene glycol) methyl ether methacrylate, M_n = 475 $gmol^{-1}$), 1,1,4,7,10,10-hexamethyltriethylene tetramine (HMTETA, 99%), copper(I) chloride (CuCl, 99%), tin chloride pentahydrate ($SnCl_4 \cdot 5H_2O$, 99%), tin (II) chloride ($SnCl_2$,

99%), ethyl cellulose, α-terpineol, 1-butylimidazole, 4-chloromethylstyrene, lithium iodide (LiI), magnesium sulfate ($MgSO_4$), 2,2′-azobisisobutyronitrile (AIBN), iodine (I_2), 3-methoxypropionitrile, butylmethylimidazolium iodide, guanidinium thiocyanate, 4-tertbutylpyridine, valeronitrile, chloroplatinic acid hexahydrate (H_2PtCl_6), and methyl orange were purchased from Sigma-Aldrich (St. Louis, MO). Tetrahydrofuran (THF), N-methyl pyrrolidone (NMP), methanol, 2-propanol, chloroform, acetonitrile, diethylether, and ethyl acetate were purchased from J.T. Baker. Deionized water (>18 MΩ·m) was obtained with a Millipore water purification system. Ruthenium dye (535-bisTBA, N719) and 60 μm-thick Surlyn were purchased from Solaronix, Switzerland. Fluorine-doped tin oxide (FTO) conducting glass substrate (TEC8, 8 ohms/sq, 2.3 mm-thick) was purchased from Pilkington, France. All chemicals and solvents reagents were of analytical grade and were used as-received without further purification.

Preparation of HM-SnO_2 spheres using graft copolymer

HM-SnO_2 spheres were prepared by the solverthermal method using tin chloride pentahydrate as a precursor and PVC-*g*-POEM graft copolymer as a structure-directing agent. PVC-*g*-POEM graft copolymer consisting of a poly(vinyl chloride) backbone and poly(oxyethylene methacrylate) side chains was synthesized *via* atomic transfer radical polymerization (ATRP) according to a previously reported method.[22,28] Typically, 0.2 g graft copolymer was dissolved in 36 mL of THF. Separately, 0.15 g of tin chloride pentahydrate was dissolved and stabilized in the mixture solution of 4 ml H_2O with vigorous stirring. After aging for 15 min, SnO_2 precursor solution was added to the graft copolymer solution. After vigorous stirring for 1 h, the solution was transferred to an autoclave and kept at 180 ℃ for 3 h and then, the autoclave was cooled naturally in air. The resultant precipitate was

centrifuged and washed with THF and ethanol three times and then dried at room temperature for further experiments and characterization. Samples were then calcined at 500^{o}C for 2 h in air to remove residual organic components. In addition, NP-SnO_2 spheres were made from tin chloride pentahydrate without graft copolymer as a control.

Preparation of HM-SnO_2 sphere photoanodes

Before deposition of the HM-SnO_2 sphere layer, clean FTO glass substrates were coated with a multi-functional om-SnO_2 IF layer solution based on a graft copolymer template, followed by calcination at 450^{o}C for 30 min.[22] Then, SnO_2 paste (HM-SnO_2 spheres or NP-SnO_2 spheres) was deposited on the om-SnO_2 IF layer-coated FTO glass using a doctor-blade technique and successive annealing at 450^{o}C for 30 min. To prepare a screen-printable viscous SnO_2 paste, 0.1 g of HM-SnO_2 spheres or NP-SnO_2 spheres was dispersed in 2 ml of ethanol with sonication for 30 min, followed by stirring for 1 h. Then, 0.5 ml of ethyl cellulose solution dissolved in ethanol at 10 wt% and 0.4 g of α-terpineol were added to the SnO_2 suspension and stirred at room temperature for 20 min, followed by sonication for 30 min. The paste was concentrated by evaporation of ethanol at room temperature for 1 day. Then, HM-SnO_2 sphere and NP-SnO_2 sphere photoanodes were sensitized with ruthenium solution (10^{-4} M) in ethanol at 50 ^{o}C for 2 h in a dark room without any post-treatment. Finally, the dye-sensitized solar cell photoanodes were immersed in absolute ethanol for 5 min to remove non-adsorbed dye on the surface.

Fabrication of DSSCs

Two types of electrolytes were used to fabricate DSSCs: 1) solid-state polymerized ionic liquid (PIL), *i.e.*, poly(1-((4 ethenylphenyl)methyl)-3-butyl-imidazolium iodide)

(PEBII) and 2) liquid electrolyte consisting of 1-butyl-3-methylimidazolium iodide, iodine (I_2), guanidinium thiocyanate, and 4-tert-butylpyridine (TBP) in acetonitrile and valeronitrile. For the ssDSSC system, PIL electrolyte solution was prepared by dissolving a PEBII solution (2 and 10 wt%) in acetonitrile. The PIL electrolyte solution infiltrated deeply into the photoanode and covered the counter electrode.[24] Cells were placed in a drying oven at 40 ℃ for 24 h and subsequently in a vacuum oven at 40 ℃ for 24 h to ensure complete solvent evaporation. Then, ssDSSCs were placed in a vacuum oven for a day to permit complete evaporation of the solvent and then sealed with an epoxy resin. In the case of the liquid system, DSSCs with liquid electrolyte were assembled using 60 μm-thick Surlyn, then the inner spaces of the DSSCs were filled with a liquid electrolyte solution through a drilled hole on the counter electrode. Liquid electrolyte solution comprised 0.6 M 1-butyl-3-methylimidazolium iodide, 0.03 M I_2, 0.1 M guanidinium thiocyanate, and 0.5 M 4-tert-butylpyridine in a mixture of acetonitrile and valeronitrile (v/v, 85:15). Pt-coated counter electrodes were prepared by spin coating of a 7 mM H_2PtCl_6 solution in isopropyl alcohol and calcination at 450 ^oC for 30 min. The photoanode active area, determined by the aperture of a black mask, was 0.16 cm^2.

Measurement of photocatalytic activity

In a typical reaction, 0.005 g of prepared photocatalyst (HM-SnO_2 spheres, NP-SnO_2 spheres) was added to 500 mL of methyl orange (MO) aqueous solution (20 mg/L) in a quartz reactor with a sealed bottom. Prior to irradiation, the solution was stirred for 30 min in the dark to stabilize and equilibrate adsorption of MO on the surface of the photocatalyst. The solution was irradiated with UV light with constant stirring to ensure homogeneity of the photocatalyst in the solution. Concentration of MO was determined using UV-Vis absorption

spectra and the maximal absorbance peak value (at 462.5 nm) was used to determine the amount of degraded MO, corresponding to the photo-activity of the catalyst. Residual MO content was calculated as C/C_o, where C and C_o are the concentrations of the tested solution.

Characterization

Morphologies, sizes, and intrinsic structures of HM-SnO_2 and NP-SnO_2 spheres were determined by FE-SEM (SUPRA 55VP, Germany, Carl Zeiss) and EF-TEM (LIBRA 120). Crystalline structures of HM-SnO_2 and NP-SnO_2 spheres were analyzed using an X-ray diffraction (XRD, Rigaku)18 kW rotating anode X-ray generator equipped with CuKα radiation (λ = 1.5406 Å). Brunauer-Emmett-Teller (BET) and Barrett–Joyner–Halenda (BJH) measurements were conducted using a using a Belsorp-mini II with N_2 as the adsorbate at liquid nitrogen temperature. In preparation for XRD measurements, TiO_2 films were degassed at 70^oC under dynamic vacuum (10^{-2} Torr) for 1 h. Diffused reflectance spectra of HM-SnO_2 and NP-SnO_2 spheres were collected in the wavelength range of 400~800 nm using a UV-visible spectrophotometer (Hewlett-Packard, Hayward, CF). IPCE system for DSSCs (K3100) was used to provide incident light with a wavelength range of 400 to 800 nm for incident photon to current conversion efficiency (IPCE) measurements. Electrochemical impedance spectroscopy (EIS) analysis was used to investigate the internal resistance at the electrode/electrolyte interface and the recombination kinetics of photoanode in DSSCs. Photoanode thickness was measured using an alpha-step IQ surface profile (KLA Tencor). Photocurrent density-voltage curves (J-V) were generated using a Keithley 2400 source meter under 1 sun illumination (AM 1.5G; 100 mW cm^{-2}) with a solar light simulator (Oriel, 91193). A NREL-calibrated Si cell with an optical filter was used to adjust the light intensity of the 1000 W xenon arc lamp that served as the light source. During photocurrent density-voltage

measurements, DSSCs were covered with a black mask with an aperture to avoid additional light coming through the lateral space. Photoelectrochemical performance was evaluated using the following equations:

$$FF = V_{max} \cdot J_{max} / V_{oc} \cdot J_{sc} \qquad (1)$$

$$\eta = V_{max} \cdot J_{max} / P_{in} \cdot 100 = V_{oc} \cdot J_{sc} \cdot FF / P_{in} \cdot 100 \qquad (2)$$

where *Jsc* is the short-circuit current density (mA/cm^2), *Voc* is the open-circuit voltage (V), Pin is the incident light power, *FF* is the fill factor, η is the overall energy conversion efficiency, and J_{max} (mA/cm^2) and V_{max} (V) are the current density and voltage in the *J*-*V* curve, respectively, at the point of maximum power output.

Results and discussion

Synthesis and characterization of HM-SnO_2 spheres

To synthesize HM-SnO_2 spheres with two pore sizes, we used PVC-*g*-POEM graft copolymer as a structure-directing agent; this copolymer can be easily synthesized via ATRP (**Scheme 1**). ATRP creates nanometer-scale organic-inorganic hybrid materials through self-assembly of graft copolymer copolymers.[28] During a solverthermal process at 180 ℃ for 3 h, a hydrophilic Sn precursor, i.e. tin chloride pentahydrate, preferentially interacts and embeds into hydrophilic POEM domains of microphase-separated PVC-*g*-POEM graft copolymer. These hybrids can subsequently be transformed into nanostructured tin oxides with mesopores by calcination of the blend. Thus, graft copolymer not only inhibits the aggregation of SnO_2 nanocrystals during the solverthermal process, but also generates mesopores with controlled porosity after calcination at 500 ^{o}C.

To improve the photovoltaic and photocatalytic performance of a photoanode, it should have a high specific surface area, good light scattering ability, excellent connectivity between nanoparticles, and sufficient electrolyte infiltration into electrode pores. In this context, we performed EF-TEM and FE-SEM measurements to further characterize the structure and morphology of HM-SnO_2 spheres. NP-SnO_2 spheres without graft copolymer were also assessed for structural comparison. Representative EF-TEM and FE-SEM images of the as-synthesized NP-SnO_2 spheres are shown in **Figs. 1a, c**; spheres were relatively smooth with an average size of 100~300 nm, and had a nonporous morphology. Formation of spherical structures is an interesting result of the solverthermal process, but NP-SnO_2 spheres are not appropriate for photovoltaic and photocatalytic applications due to their low surface area resulting from their lack of pores. Incorporation of the graft copolymer into the Sn precursor solution yielded HM-SnO_2 spheres with higher porosity, a larger surface area, and better interconnectivity than the NP-SnO_2 spheres (**Figs. 1b, d**). Secondary colloidal spheres with a diameter between 100~300 nm formed; these consisted of numerous primary nanoparticles of 15 nm in diameter, which could enhance light scattering. These results indicated that PVC-*g*-POEM graft copolymer played a significant role as a structure-directing agent to control the agglomeration of Sn precursor during the solverthermal process. Well-interconnected, porous HM-SnO_2 structures consisting of small particles aggregated into larger clusters were obtained; we expected this combination of small particles and larger clusters to result in a synergistic improvement in light harvesting, electron transport, electrolyte penetration, and consequently photovoltaic and photocatalytic performance.

Phase structure and crystallite size of nanoscale metal oxides have a significant effect on photovoltaic and photocatalytic performance. Thus, we characterized NP-SnO_2 and HM-SnO_2 spheres by X-ray diffraction; results are shown in **Fig. 2**. Crystallite size was estimated

using the following Scherrer formula:

$$D = k\lambda / \beta \cos\theta \qquad (3)$$

where D is the crystalline SnO_2 nanocrystalline size, k is a shape factor of the nanocrystalline (0.89), λ is the wavelength of the X-rays (1.5406 Å), β is the full width of the diffraction peak at half maximum intensity (FWHM), and θ is half of Bragg's diffraction angle of the centroid of the peak in degrees.[29] Both NP-SnO_2 and HM-SnO_2 spheres exhibited sharp diffraction peaks at 26.8°, 34.0°, 38.1°, 52.1°, and 54.7°, which have been assigned to reflections from the (110), (101), (200), (211), and (220) planes, respectively, of the rutile SnO_2 phase (ICDD-JCPDS card no. 41-1445).[30] These results demonstrated that structural changes and phase transformation of the Sn precursor to crystalline rutile SnO_2 occurred *via* a solverthermal process at 500 °C. However, broadening of the diffraction peaks was significantly different between NP-SnO_2 spheres and HM-SnO_2 spheres, related to their different crystallite sizes. The average crystallite size of HM-SnO_2 spheres was approximately 17.6 nm, which was much smaller than that of NP-SnO_2 spheres (127.2 nm). This is because the HM-SnO_2 spheres comprised a number of primary small particles with a crystallite size of 10-20 nm that aggregated into large clusters, whereas NP-SnO_2 spheres consisted only of nonporous large clusters with a crystallite size of 100-200 nm, as confirmed by the EF-TEM and FE-SEM images shown in **Fig. 1**.

Performance of photovoltaic and photocatalytic applications is strongly dependent on both the surface area and porosity of nanoscale metal oxides. Thus, N_2 absorption-desorption measurements were taken to investigate the surface area and porosity of NP-SnO_2 and HM-SnO_2 spheres, as shown in **Fig. 3**. Specific surface area was calculated using the BET method,

while average pore diameter was determined using the BJH method. Specific surface area of NP-SnO_2 spheres was low at 37.2 m^2 g^{-1}. Based on the BJH pore size distribution curves, we concluded that pores with a size of 100~200 nm were dominant in NP-SnO_2 spheres, consistent with the FE-SEM and TEM results. Specific surface area of HM-SnO_2 spheres was determined to be 85.3 m^2 g^{-1}, which is approximately 2.3-fold higher than that of the NP-SnO_2 spheres. In addition, HM-SnO_2 spheres exhibited a Type IV N_2 isotherm loop (according to the IUPAC classification) where the hysteresis loop approached relatively higher pressures, indicating the presence of an interconnected mesoporous structure. Particularly, tailing upward at a higher hysteresis loop relative pressure (i.e. $P/P_0 = 1$) indicated the formation of a macroporous structure, with the contribution of large pores beyond the mesopore scale. HM-SnO_2 spheres showed a remarkable bimodal pore structure with mesopores 23.5 nm in diameter and macropores 162.3 nm in diameter. This indicated that PVC-g-POEM graft copolymer controlled the agglomeration of Sn precursor as a structure-directing agent. It should be noted that the specific surface area of commercially available nanocrystalline SnO_2 is 23.1 m^2 g^{-1}, which is much smaller than that of the HM-SnO_2 spheres.[31] Furthermore, the specific surface area of the HM-SnO_2 spheres (85.3 m^2 g^{-1}) was larger than those of previously reported SnO_2 mesoporous nanostructures (78.2 m^2 g^{-1} and 43 m^2 g^{-1}).[25-27] We predicted that these HM-SnO_2 spheres would promote greater generation of photoelectrons, allow facile transport of the electrolyte, and enhance photovoltaic and photocatalytic device performance compared to previously reported SnO_2 mesoporous nanostructures.

Photovoltaic performance of DSSCs

Because the performance of photovoltaic applications is strongly dependent on light-

scattering by photoanodes, we measured the UV-visible reflectance spectra of an as-prepared HM-SnO_2 sphere layer with and without N719 dye sensitizer, as shown in **Figs. 4a, b**. We used a NP-SnO_2 sphere layer as a control. We also used a multi-functional om-SnO_2 IF layer as a buffer layer because this structure has been previously shown to enhance light harvesting, improve electron transport by suppression of recombination or back-reactions, and reduce interfacial/internal resistance, yielding high-performance DSSCs with good long-term stability.[22] As observed in the plan-view FE-SEM image (**Fig. S1a**), the om-SnO_2 IF layer consisted of tightly adhered nanoparticles without any structural defects and showed excellent interconnectivity and well-ordered porosity. The om-SnO_2 IF layer was approximately 500 nm-thick, and adhered tightly to the FTO glass with good interfacial contacts (**Fig. S1b**). As shown in **Fig. 4a**, high reflectance values above 50% were observed for both HM-SnO_2 and NP-SnO_2 spheres layer without N719 dye sensitizer in the visible light wavelength range of 400~800 nm, indicating excellent light-scattering ability. It should be noted that the less-organized, commercially available nanocrystalline SnO_2 photoanode showed a reflectance value below 20 % over the entire wavelength regions (**Fig. S2**). On the other hands, after N719 dye sensitizer adsorption, the reflectance of the HM-SnO_2 sphere layer was reduced to 20% in the 400~500 nm wavelength region, which is much lower than that of the NP-SnO_2 sphere layer (~ 40%), as shown in **Fig. 4b**. These results can be explained by the fact that the presence of aggregated, large nanostructures improved light scattering, leading to an increase in red light harvesting. Primary small nanoparticles in HM-SnO_2 spheres provided a large specific surface area for dye adsorption; we therefore also expected to observe an increase in the short circuit current (J_{sc}).

IPCE is defined as the ratio of the number of electrons in the external circuit produced by an incident photon at a given wavelength. Therefore, light-harvesting ability can be

evaluated by measuring the IPCE spectra of a device. IPCE values of ssDSSCs fabricated with NP-SnO_2 and HM-SnO_2 spheres on a multi-functional om-SnO_2 IF layer are shown in **Fig. 5** as a function of illumination wavelength. PEBII was synthesized via free radical polymerization and employed as a solid electrolyte. This obviated the need for incorporation of additives such as I_2, ionic liquids, and salts.[32] ssDSSCs fabricated with HM-SnO_2 on a multi-functional om-SnO_2 IF layer had significantly higher absolute IPCE values than ssDSSCs fabricated with NP-SnO_2 sphere cells over the whole spectral range, which we attributed to the superior light harvesting ability of HM-SnO_2 spheres (**Fig. 5a**). Light-scattering effect was greater for longer wavelengths (> 520 nm) because more light was transmitted through the photoanode and scattered in this region.[33] Spectrally selective enhancement for these two systems was considerable, as shown in **Fig. 5b**. Notably, the normalized IPCE value of ssDSSCs based on the HM-SnO_2 sphere system showed a significant broadening below 520 nm as compared with the NP-SnO_2 sphere system. Such broadening of the spectral domain indicated improved light harvesting in this wavelength region, which we attributed to enhanced dye loading due to the large specific surface area of the HM-SnO_2 system, which increased photoelectrical response. The high IPCE value of ssDSSCs based on HM-SnO_2 spheres indicated that these ssDSSCs had superior light reflectance and dye loading characteristics than ssDSSCs based on NP-SnO_2 spheres.

The mechanism underlying the photovoltaic performance improvement in the HM-SnO_2 spheres on a multi-functional om-SnO_2 IF layer based ssDSSCs was further investigated by measuring the recombination resistance (R_{rec}) and electron lifetime (τ_n) of the devices as a function of bias voltage as shown in **Fig. 6**. The electron lifetime (τ_n) was derived from the product between the resistance of recombination and the capacitance for the electron transfer. Larger recombination resistance and longer electron lifetime were obtained in the HM-SnO_2

spheres on a multi-functional om-SnO_2 IF layer based ssDSSCs, indicating increased electron transport and reduced interfacial charge recombination loss. It indicates the importance of an organized HM-SnO_2 spheres structure for electron transport, which is attributed to the good interconnectivity resulting in the improved interfacial contact of the electrode/electrolyte. And, our suggestions about the relationship between hierarchical organized structure and electron transport are consistent with a previous study by the Jiang group.[34]

We next investigated the performance of ssDSSCs with HM-SnO_2 spheres on a multi-functional om-SnO_2 IF layer as photoanode and solid-state electrolyte. Photocurrent density-voltage (*J*-*V*) characteristics are shown in **Fig. 7**. **Table 1** summarizes photovoltaic parameters such as V_{oc}, J_{sc}, fill factor (*FF*), and light-to-electricity conversion efficiency (η). In addition, reference devices were fabricated using NP-SnO_2 spheres on a multi-functional om-SnO_2 IF layer as the photoanode material. As expected, V_{oc} and J_{sc} values for ssDSSCs with HM-SnO_2 spheres were much higher than those for ssDSSCs based on NP-SnO_2 spheres. Notably, devices with photoanodes comprising HM-SnO_2 spheres on a multi-functional om-SnO_2 IF layer had a V_{oc} of 0.56 V, J_{sc} of 10.7 mA/cm^2, and *FF* of 0.57, resulting in an η of 3.4%, which is much higher than the η of the NP- SnO_2 sphere system (1.9%). This value is one of the highest reported for SnO_2-based ssDSSCs employing a solid-state electrolyte and N719 ruthenium dye as the sensitizer.

One possible reason for the enhanced V_{oc} value is suppression of charge recombination and electron back-reactions in the well-interconnected HM-SnO_2 sphere system. V_{oc} is strongly dependent on recombination or back-reactions, and a higher V_{oc} value can be attained by suppressing those reactions as reflected by the following equation:

$$V_{oc} = (RT / nF) \cdot ln\,(AI / (n_o k_1(I_3^-) + n_0 k_2(D^+))) \qquad (4)$$

where R is the molar gas constant, T is the temperature, F is the Faraday constant, n is the reaction order for triiodide (I_3^-) and electrons, A is the electrode area, I is the incident photon flux, n_o is the concentration of accessible electron states in the conduction band, and k_1 and k_2 are the kinetic constants of the back reaction of the injected electrons with triiodide (I_3^-) and the recombination of these electrons with oxidized dyes (D^+), respectively.[35] Electron lifetime (τ_n) of a photoanode comprising HM-SnO_2 spheres on a multi-functional om-SnO_2 IF layer was higher than that of a photoanode based on NP-SnO_2 spheres. This indicates more effective electron transport and reduced electron trapping for charge recombination in the former system, which could further increase the V_{oc} value. J_{sc} value is related to light harvesting, electron injection, and electron collection, and can be calculated using the following equation:

$$J_{sc} = q \cdot \eta_{lh} \cdot \eta_{inj} \cdot \eta_{col} \cdot I_0 \qquad (5)$$

where q is the elementary charge, η_{lh} is the light harvest efficiency of a cell, η_{inj} is the electron injection efficiency, η_{col} is the electron collection efficiency, and I_0 is the light flux.[36] We attributed the improved J_{sc} value of the HM-SnO_2 spheres on a multi-functional om-SnO_2 IF layer to the presence of well-interconnected secondary aggregated nanostructures that improved light harvesting by providing a large specific surface area for dye loading, increasing light scattering, and improving electron collection efficiency (see the Supporting Information, **Table S1**). *FF* values were not significantly different between the two systems. This is because both NP-SnO_2 and HM-SnO_2 sphere photoanodes possessed large micropores of 100 – 200 nm size as confirmed by BET and SEM analysis, which allowed for facile pore

infiltration of solid-state electrolyte without perturbation of cell kinetics.

DSSCs were also fabricated with a liquid state electrolyte containing iodine (I_2), 1-butyl-3-methylimidazolium iodide, guanidinium thiocyanate, and 4-tert-butylpyridine in a mixture of acetonitrile and valeronitrile. *J-V* curves for these DSSCs are shown in **Fig. S3** and their photovoltaic parameters are summarized in **Table 1.** A J_{sc} of 12.3 mA/cm^2, V_{oc} of 0.58 V, *FF* of 0.58, and a η of 3.7% were obtained for DSSCs based on HM-SnO_2 spheres and a multi-functional om-SnO_2 IF layer under 1 sun illumination (AM 1.5G; 100 mW cm^{-2}). This efficiency is high compared to that of DSSCs with a SnO_2 photoanode and liquid state electrolyte.[17,37]

ssDSSCs fabricated without a multi-functional om-SnO_2 IF layer exhibited an efficiency of only 1.7% at 100 mW/cm^2, as shown in **Fig. 7b** and **Table 2.** This result again indicates the importance of an anti-reflective, cascadal energy band gap, good interconnectivity, and high electrical conductivity.[22] We also measured the long-term stability of ssDSSCs comprising HM-SnO_2 spheres on a multi-functional om-SnO_2 IF layer photoanode with solid state electrolyte; results are shown in **Fig. S4**. Energy conversion efficiency of these ssDSSCs decreased very slowly, and efficiency remained close to the initial value even up to 30 days. This implies that our SnO_2-based device with solid-state electrolyte has a stable dye/photoanode/electrolyte interface, resulting in significantly enhanced long-term stability.

Photocatalytic performance

To evaluate the photocatalytic performance of the HM-SnO_2 spheres, we evaluated the oxidation of methyl orange under UV light irradiation. For comparison, we also evaluated the photocatalytic performance of NP-SnO_2 spheres. Before UV light illumination, colloidal

suspensions of the two types of SnO_2 spheres and methyl orange were stirred in the dark for 30 min to ensure that organic pollutants was adsorbed to saturation on the inner and outer surfaces of the catalyst. NP-SnO_2 spheres were not able to fully degrade the methyl orange molecules after 60 min of UV light irradiation, as shown in **Fig. 8a**. However, methyl orange was completely decomposed in the presence of HM-SnO_2 spheres after only 40 min of irradiation with UV light. It should be noted that HM-SnO_2 spheres showed much greater activity than Degussa P25 (See **Fig. S5**). We attributed the superior photocatalytic performance of HM-SnO_2 spheres to the presence of secondary aggregated nanostructures composed of primary small nanoparticles with a high surface area, which favored efficient light harvesting *via* enhanced methyl orange molecule loading and good light reflection. Their pseudo-first-order kinetic rate plots in **Fig. S6** indicate that HM-SnO_2 spheres have the excellent enhanced photocatalytic activity. In addition, we performed a reutilization experiment to evaluate the stability of HM-SnO_2 spheres as photocatalysts. When the photocatalytic experiment was completed, the residue was centrifuged and placed in an oven at 50^{o}C for a day. Then, the residue was dispersed in methyl orange solution and the photocatalytic experiment was repeated. As shown in **Fig. 8b**, there was only a slight decrease in the photocatalytic performance of HM-SnO_2 spheres after five cycles, demonstrating that these spheres have good photocatalytic stability.

Conclusions

In summary, we prepared HM-SnO_2 spheres by solvothermal reaction with PVC-g-POEM graft copolymer as a structure-directing agent and investigated their photovoltaic and photocatalytic performance. om-SnO_2 IF layer was used a buffer layer between the HM-SnO_2 spheres and the FTO substrates in DSSCs to improve light harvesting, enhance electron

transport, decrease charge recombination, and reduce interfacial/internal resistance. ssDSSCs fabricated with a photoanode comprising HM-SnO_2 spheres on an om-SnO_2 IF layer with the solid electrolyte of PEBII exhibited an energy conversion efficiency of 3.4% at 100 mW/cm^2, which was much higher than that attained with the NP-SnO_2 sphere system (1.9%). We attributed the outstanding improvement in photovoltaic performance to an increase in specific surface area, improved light scattering, and excellent pore filling by the solid-state electrolyte. Higher specific surface area and better light scattering ability of HM-SnO_2 spheres compared to NP-SnO_2 spheres contributed to the enhanced photocatalytic activity and good recycling performance of the former. These results can guide future designs of hierarchical mesoporous structures to realize further photovoltaic and photocatalytic improvements.

Acknowledgements

This work was supported by the Korea Center for Artificial Photosynthesis (KCAP) (2009-0093883), the Energy Efficiency & Resources of the Korea Institute of Energy Technology Evaluation and Planning (KETEP) (20122010100040) and the Converged Energy Materials Research Center program of Defense Acquisition Program Administration and Agency for Defense Development.

Reference

1 B. O'Regan and M. Gratzel, *Nature*, 1991, **353**, 737.

2 J. Liang, G. Zhang, H. Xia and Wentao Sun, *RSC Adv.***,** 2014, **4**, 12649.

3 Y. Xiao, J. Wu, G. Yue, J. Lin, M. Huang, L. Fan and Z. Lan, *RSC Adv.***,** 2012, **2**, 10550.

4 L. Chen, Y. Zhou, H. Dai, Z. Li, T. Yu, J. Liu and Z. Zou, *J. Mat. Chem. A*, 2013, **1**, 11790.

5 S. Cai, G. Tian, X. Li, J. Su and H. Tian, *J. Mat. Chem. A*, 2013, **1**, 11295.

6 G. D. Sharma, D. Daphnomili, K. S. V. Gupta, T. Gayathri, S. P. Singh, P. A. Angaridis, T. N. Kitsopoulos, D. Tasis and A. G. Coutsolelos, *RSC Adv.***,** 2013, **3**, 22412.

7 K. Yu, Z. Wen, H. Pu, G. Lu, Z. Bo, H. Kim, Y. Qian, E. Andrew, S. Mao and J. Chen, *J. Mat. Chem. A*, 2013, **1**, 188.

8 P.-W. Chen, C.-P. Lee, L.-Y. Chang, J. Chang, M.-H. Yeh, L.-Y. Lin, R. Vittal, J.-J. Lin and K.-C. Ho**,** *RSC Adv.***,** 2013, **3**, 5871.

9 Y.-F. Chan, C.-C. Wang and C.-Y. Chen, *J. Mat. Chem. A*, 2013, **1**, 5479.

10 F. Bella, J. R. Nair and C. Gerbaldi, *RSC Adv.***,** 2013, **3**, 15993.

11 J. Burschka, N. Pellet, S.-J. Moon, R. Humphry-Baker, P. Gao, M. K. Nazeeruddin and M. Gratzel, *Nature*, 2013, **499**, 316.

12 H.-Z. Chen, Y.-Y. Zhang, X. Gong and H. Xiang, *J. Phys. Chem. C*, 2014, **118**, 2333.

13 H. J. Snaith and C. Ducati, *Nano Lett.*, 2010, **10**, 1259.

14 X. Hou, Y. Hu, H. Jiang, J. Huo, Y. Li and C. Li, *J. Mat. Chem. A*, 2013, **1**, 13814.

15 E. N. Kumar, R. Jose, P. S. Archana, C. Vijila, M. M. Yusoff and S. Ramakrishna, *Energy Environ. Sci.*, 2012, **5**, 5401.

16 A. Birkel, Y.-G. Lee, D. Koll, X. V. Meerbeek, S. Frank, M. J. Choi, Y. S. Kang, K. Char and W. Tremel, *Energy Environ. Sci.*, 2012, **5**, 5392.

17 L. Cojocaru, C. Olivier, T. Toupance, E. Sellier and L. Hirsch, *J. Mater Chem. A* 2013, **1**, 13789.

18 W.-Y. Cheng, J. R. Deka, Y.-C. Chiang, A. Rogeau and S.-Y. Lu, *Chem. Mat.*, 2012, **24**, 3255.

19 Z. Li, Y. Zhou, G. Xue, T. Yu, J. Liu and Z. Zou, *J. Mat. Chem.*, 2012, **22**, 14341.

20 J. Pan, J. Li, Z. Yan, B. Zhou, H. Wu and X. Xiong, *Nanoscale*, 2013, **5**, 3022.

21 L.-P. Zhu, N.-C. Bing, D.-D. Yang, Y. Yang, G.-H. Liao and L.-J. Wang, *CrystEngComm*,

2011, **13**, 4486.

22 J. T. Park, S. H. Ahn, D. K. Roh, C. S. Lee and J. H. Kim, *ChemSusChem*, DOI: 10.1002/cssc.201301215.

23 Y. J. Kim, K. H. Kim, P. Kang, H. J. Kim, Y. S. Choi and W. I. Lee, *Langmuir*, 2012, **28**, 10620.

24 J. T Park, W. S. Chi, D. K. Roh, S. H. Ahn and J. H. Kim, *Adv. Funct. Mat.*, 2013, **23**, 26.

25 X. Wang, S. Qiu, J. Liu, C. He, G. Lu and W. Liu, *Eur. J. Inorg. Chem.*, 2014, **2014**, 863.

26 X. Wang, S. Qiu, C. He, G. Lu, W. Liu and J. Liu, *RSC Adv.*, 2013, **3**, 19002.

27 X. Yin, L. Chen, C. Li, Q. Hao, S. Liu, Q. Li, E. Zhang and T. Wang, *Electrochimica Acta, 2011*, **56**, 2358.

28 D. K. Roh, S. J. Kim, H. Jeon and J. H. Kim, ACS Appl. Mater. Interfaces, 2013, **5**, 6615.

29 K. Zhu, N. R. Neale, A. Miedaner and A. J. Frank, *Nano Lett.*, 2007, **7**, 69.

30 ICDD-JCPDS database, no. 41-1445

31 J. Qian, P. Liu, Y. Xiao, Y. Jiang, Y. Cao, X. Ai and H. Yang, *Adv. Mat.*, 2009, **21**, 3663.

32 J. T. Park, J. H. Prosser, S. H. Ahn, S. J. Kim, J. H. Kim and D. Lee, *Adv. Funct. Mat.*, 2013, **23**, 2193.

33 J. T. Park, D. K. Roh, R. Patel, E. Kim, D. Y. Ryu and J. H. Kim, *J. Mat. Chem.*, 2010, **20**, 8521.

34 D. Wu, Z. Gao, F. Xu, J. Chang, W. Tao, J. He, S. Gao and K. Jiang, *CrystEngComm*, 2013, **15**, 1210.

35 J. T. Park, W. S. Chi, H. Jeon and J. H. Kim, *Nanoscale*, 2014, **6**, 2718.

36 P. Tiwana, P. Docampo, M. B. Johnston, H. J. Snaith and L. M. Herz. *ACS nano*, 2011, **5**, 5158.

37 Z. Li, Y. Zhou, J. Song, T. Yu, J. Liu and Z. Zou, *J. Mat. Chem. A*, 2013, **1**, 524.

Scheme and figure captions

Scheme 1. Schematic representation of the preparation of hierarchical mesoporous SnO_2 (HM-SnO_2) and nonporous SnO_2 (NP-SnO_2) spheres, synthesized with and without PVC-g-POEM graft copolymer as a structure-directing agent, respectively.

Figure 1. EF-TEM images of (a) NP-SnO_2 spheres, (b) HM-SnO_2 spheres and (c) FE-SEM images of NP-SnO_2 spheres, (d) HM-SnO_2 spheres.

Figure 2. X-ray diffraction patterns of NP-SnO_2 spheres and HM-SnO_2 spheres.

Figure 3. (a) BET N_2 adsorption-desorption isotherms and (b) BJH pore size distribution curves of NP-SnO_2 spheres and HM-SnO_2.

Figure 4. Reflectance spectra of a NP-SnO_2 sphere layer and HM-SnO_2 sphere layer on multi-functional om-SnO_2 IF layer-coated FTO glass (a) without and (b) with N719 dye sensitizer.

Figure 5. (a) Absolute and (b) normalized IPCE spectra of ssDSSCs fabricated with NP-SnO_2 spheres and HM-SnO_2 on a multi-functional om-SnO_2 IF layer photoanode with a solid electrolyte of poly(1-((4-ethenylphenyl)methyl)-3-butyl-imidazolium iodide) (PEBII).

Figure 6. (a) Recombination resistance (R_{rec}) and (b) electron lifetime (τ_n) of ssDSSCs fabricated with NP-SnO_2 spheres and HM-SnO_2 spheres on a multi-functional om-SnO_2 IF layer photoanode.

Figure 7. Photocurrent density-voltage curve of (a) ssDSSCs based on NP-SnO_2 spheres and HM-SnO_2 spheres on a multi-functional om-SnO_2 IF photoanode layer and (b) ssDSSCs based on HM-SnO_2 spheres with and without a multi-functional om-SnO_2 IF layer under 1 sun illumination (AM 1.5G; 100 mW cm^{-2}).

Figure 8. (a) Photocatalytic reactions of NP-SnO_2 spheres and HM-SnO_2 spheres with methyl orange under UV irradiation, (b) photocatalytic recycling test of HM-SnO_2 spheres.

Scheme 1

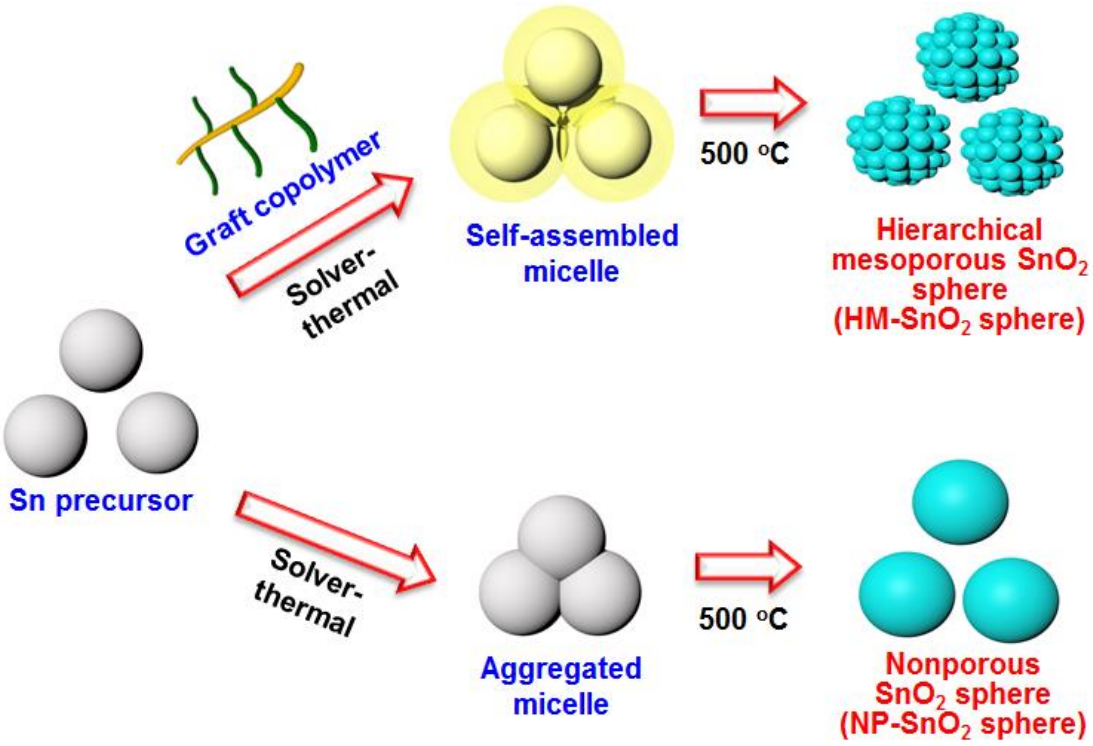

Figure 1

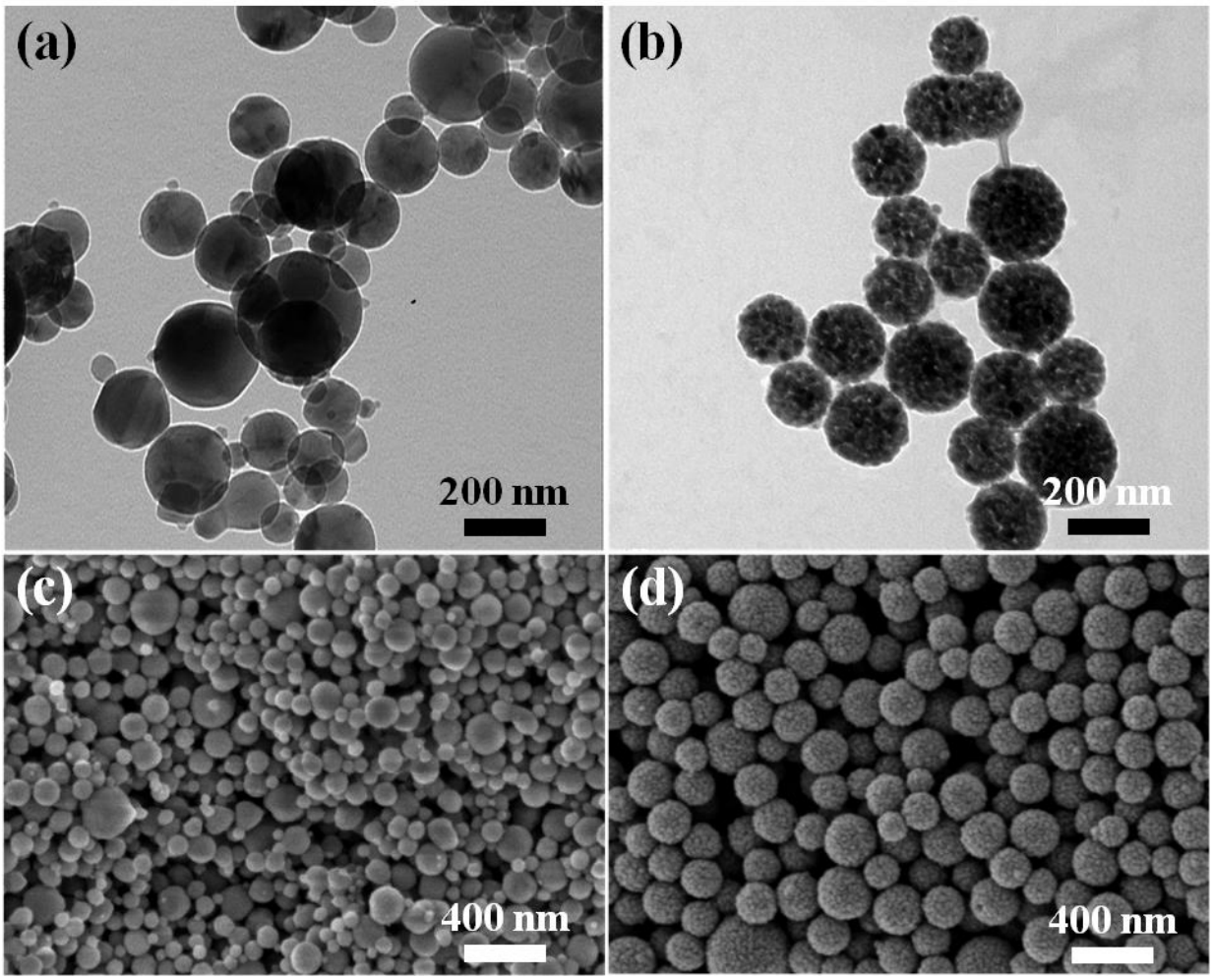

Figure 2

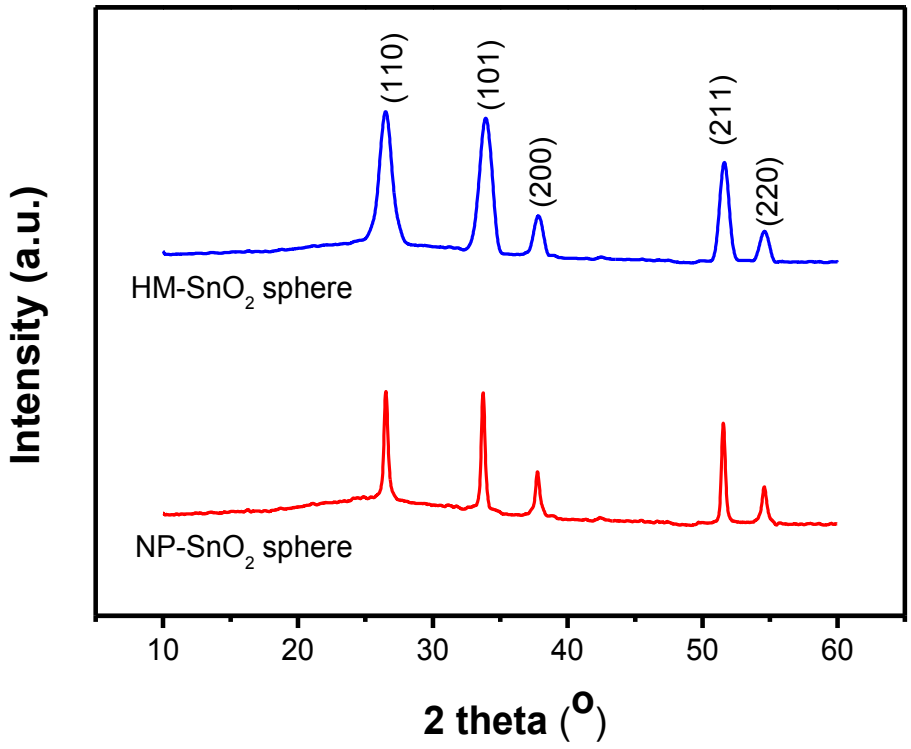

Figure 3

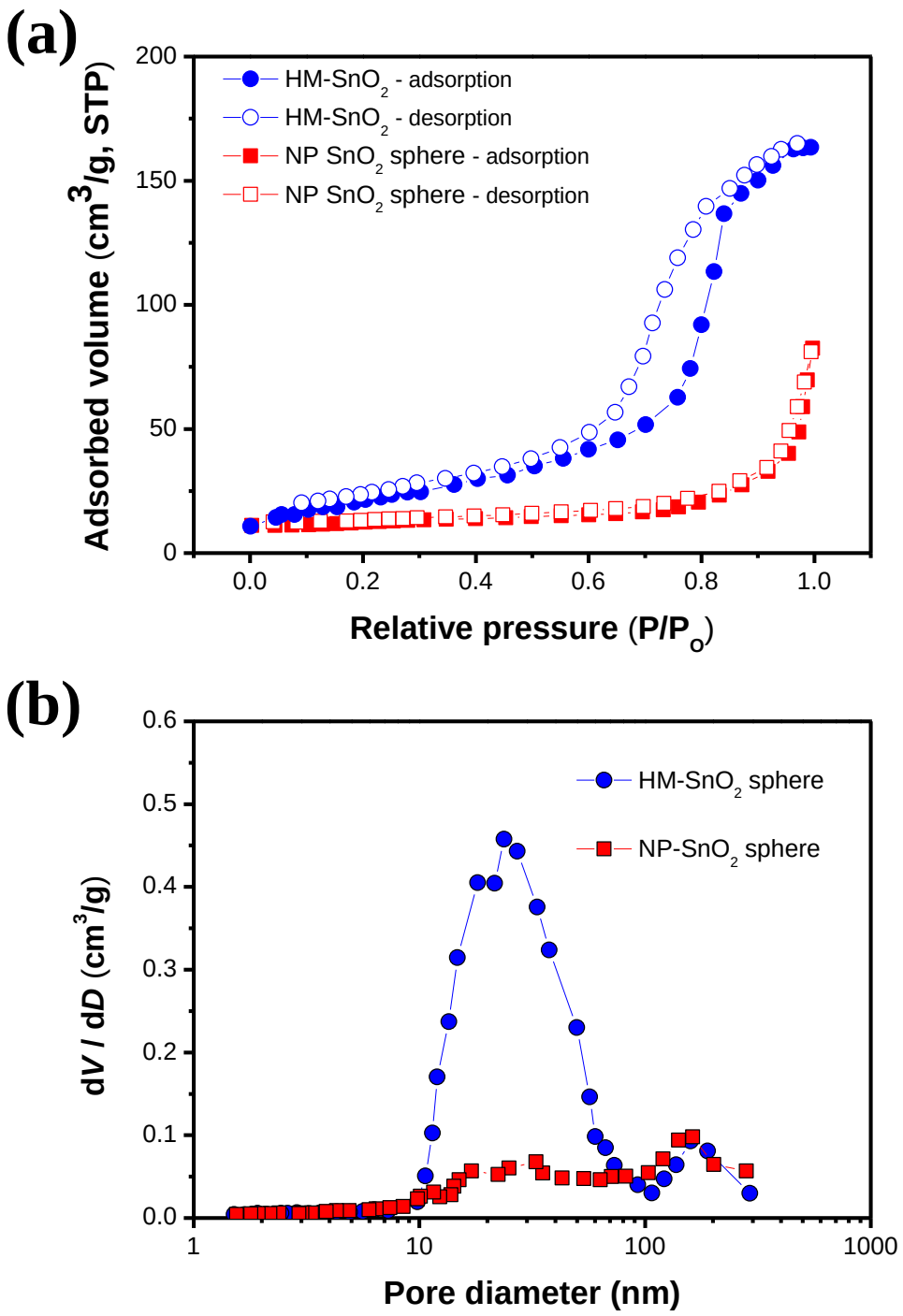

Figure 4

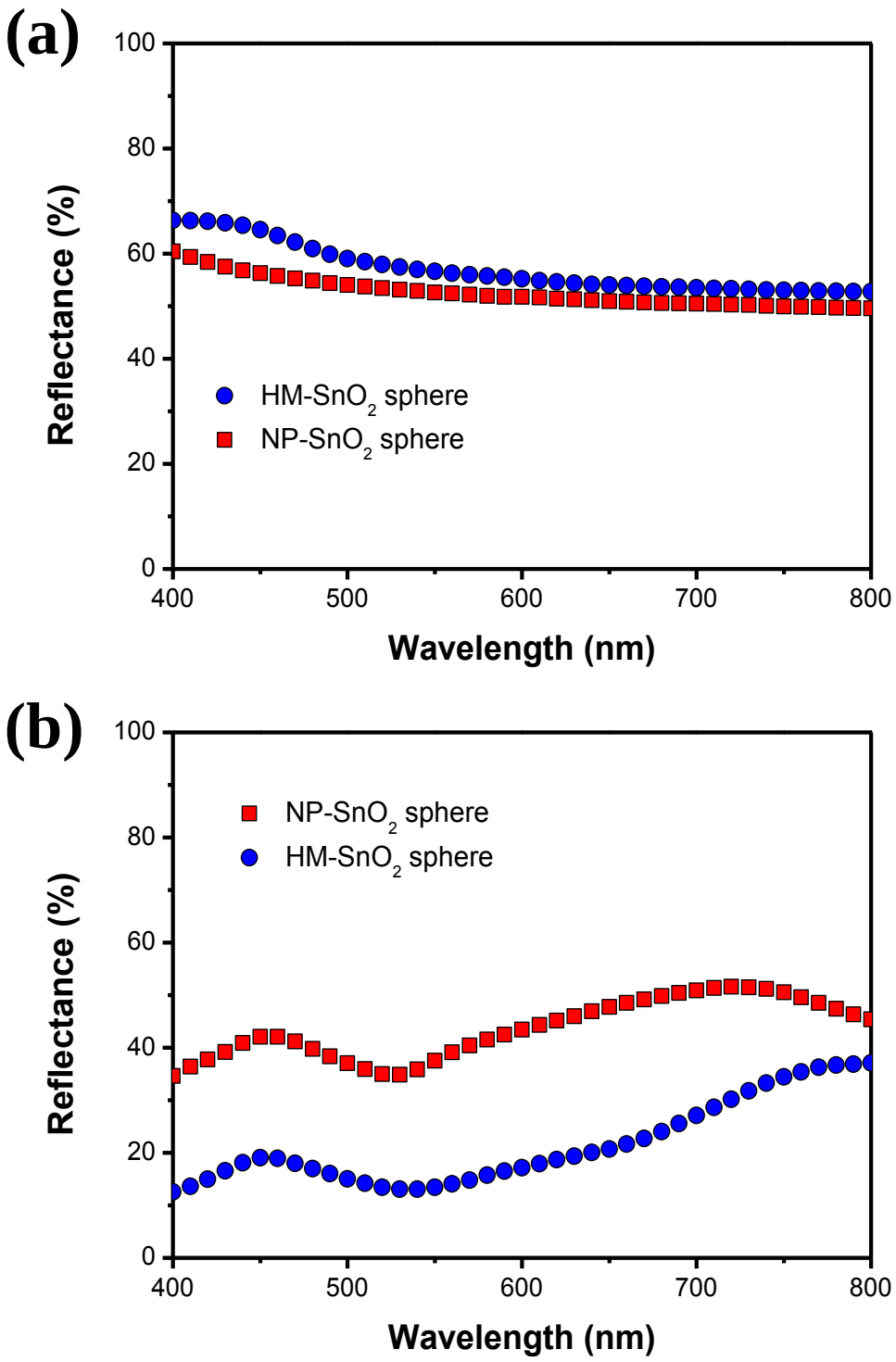

Figure 5

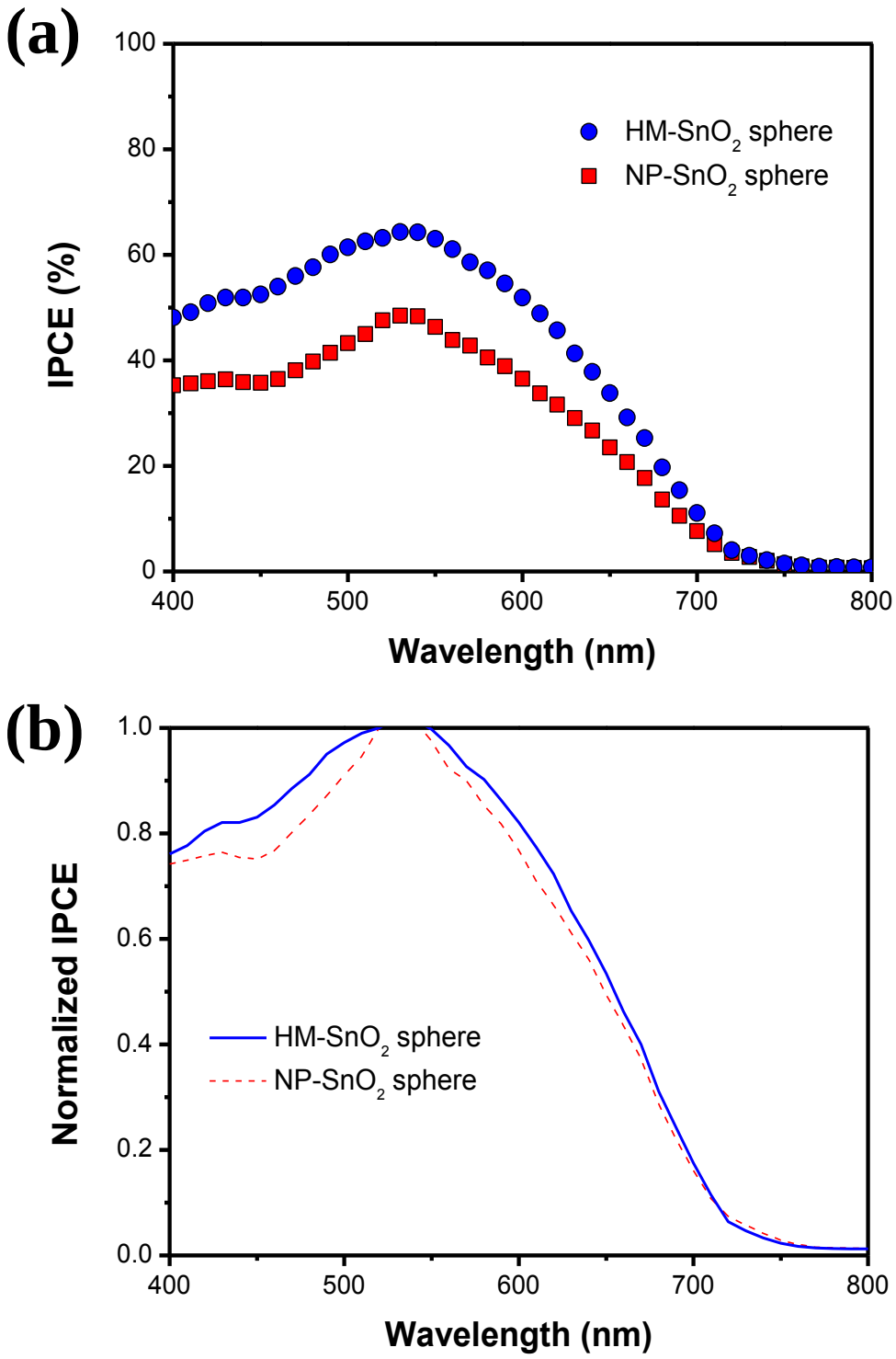

Figure 6

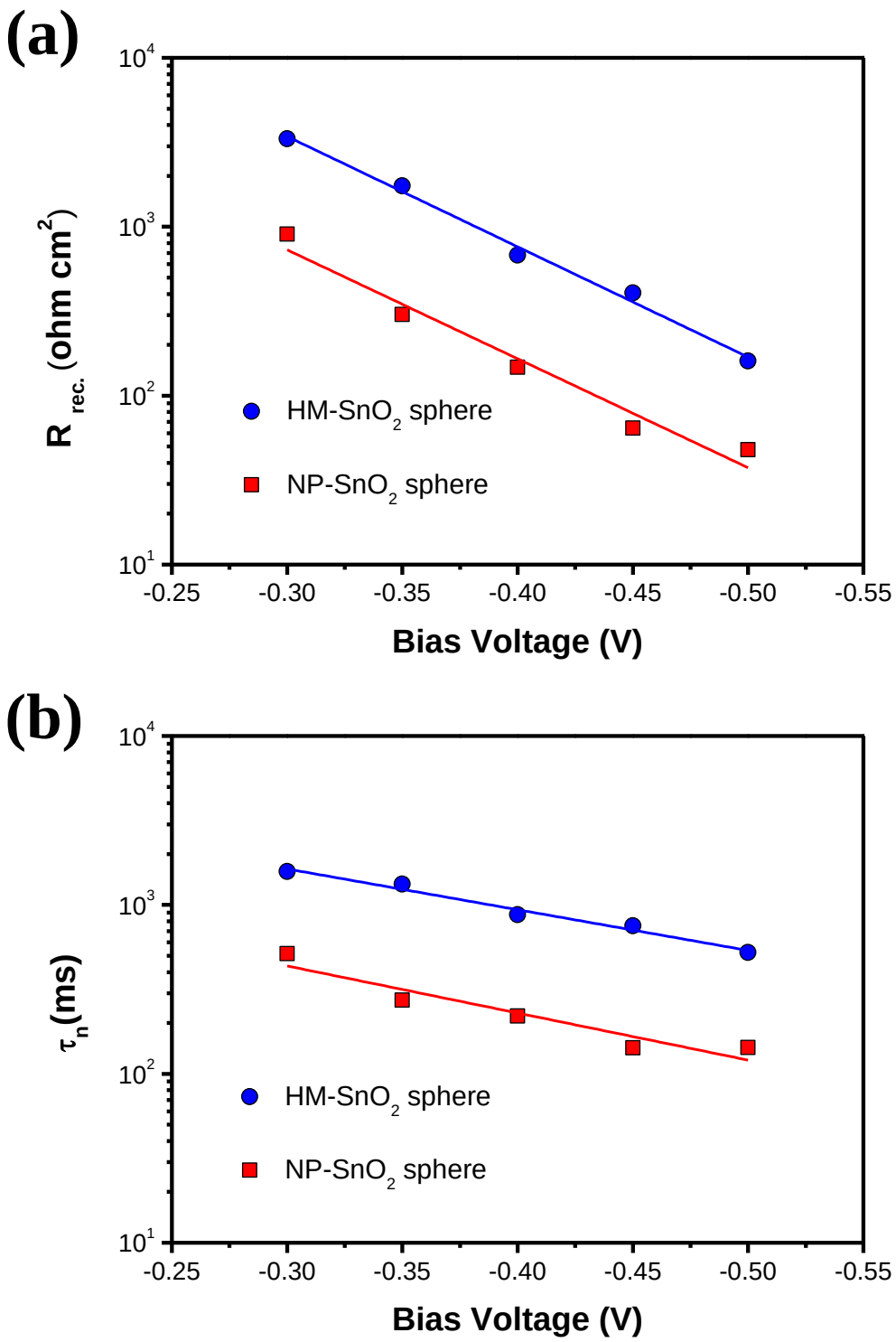

Figure 7

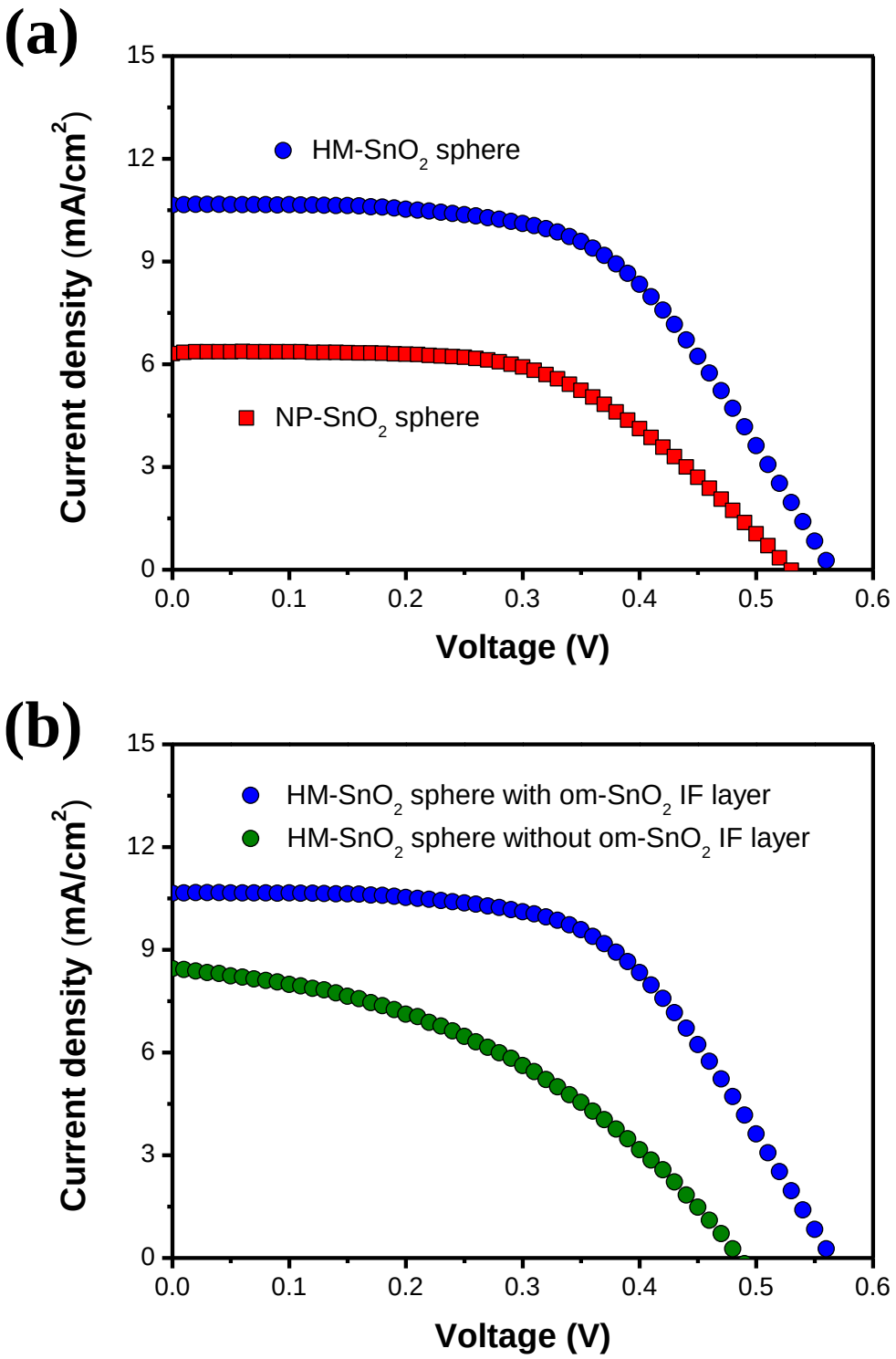

Figure 8

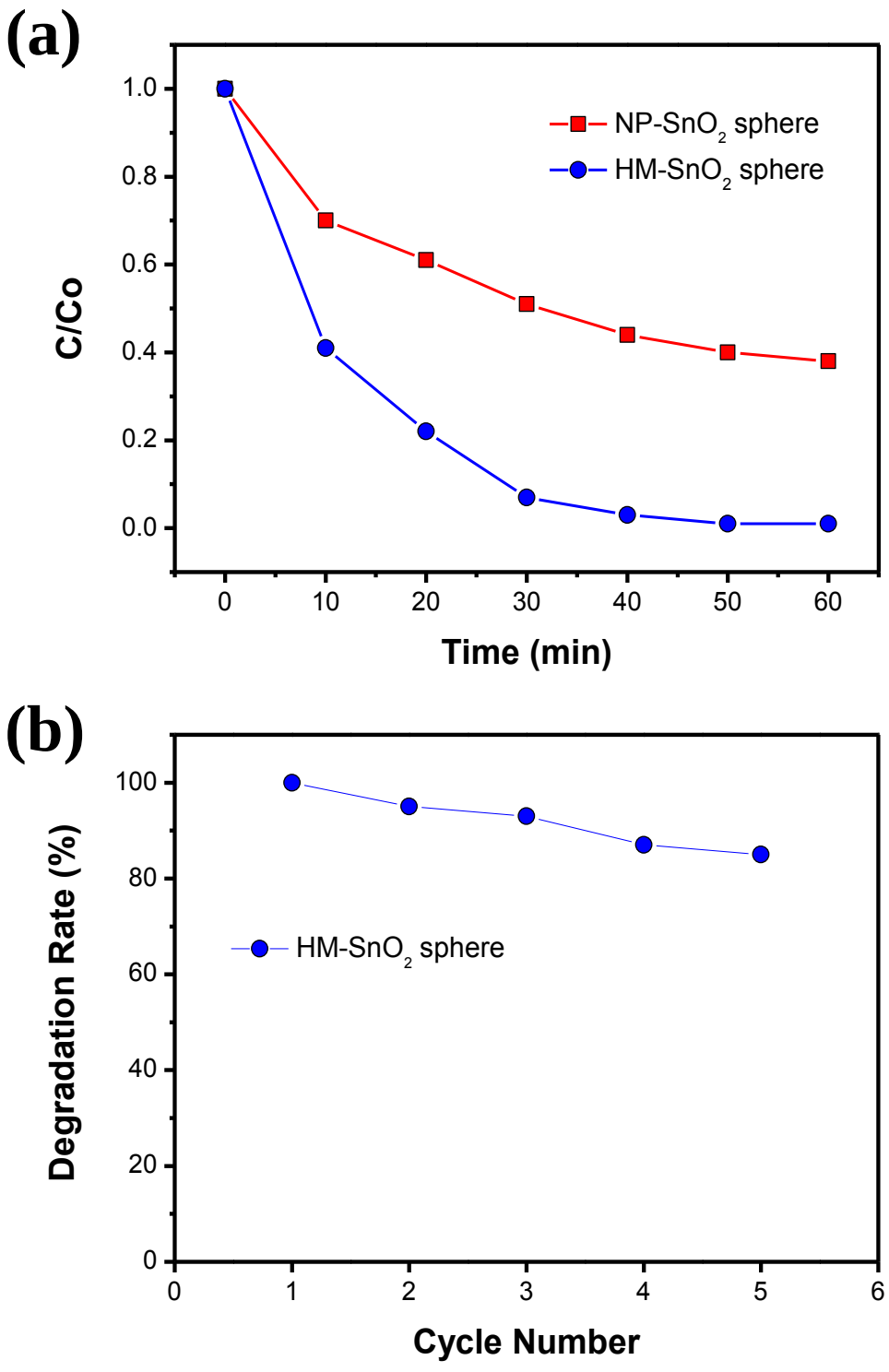

Table 1. Photovoltaic parameters of DSSCs fabricated using NP-SnO_2 spheres and HM-SnO_2 spheres on a multi-functional om-SnO_2 IF photoanode layer with solid and liquid state electrolytes at 100 mW/cm^2.[a,b] Total thickness of the photoanode was approximately 10 μm.

Photoanode	Electrolyte	V_{oc} (V)	J_{sc} (mA/cm^2)	*FF*	η (%)
NP-SnO_2 spheres/om-SnO_2 IF layer	Solid	0.52	6.3	0.56	1.9
	Liquid	0.49	7.8	0.58	2.2
HM-SnO_2 spheres/om-SnO_2 IF layer	Solid	0.56	10.7	0.57	3.4
	Liquid	0.52	12.3	0.58	3.7

[a] Solid electrolyte: poly(1-((4ethenylphenyl)methyl)-3-butyl-imidazolium iodide)) (PEBII).

[b] Liquid electrolyte: 1-butyl-3-methylimidazolium iodide, I_2, guanidinium thiocyanate, and 4-tert-butylpyridine in a mixture of acetonitrile and valeronitrile.

Table 2. Photovoltaic parameters of ssDSSCs fabricated using HM-SnO_2 spheres with and without a multi-functional om-SnO_2 IF layer with solid electrolyte at 100 mW/cm^2.

Photoanode	V_{oc} (V)	J_{sc} (mA/cm^2)	*FF*	η (%)
HM-SnO_2 spheres without an om-SnO_2 IF layer	0.48	8.5	0.42	1.7
HM-SnO_2 spheres with an om-SnO_2 IF layer	0.56	10.7	0.57	3.4

Supporting Information

One-pot Synthesis of Hierarchical Mesoporous SnO_2 Spheres Using Graft Copolymer: Enhanced Photovoltaic and Photocatalytic Performance

Jung Tae Park,[a,b] Chang Soo Lee,[a] Jong Hak Kim[a,*]

[a] *Department of Chemical and Biomolecular Engineering, Yonsei University, 262 Seongsanno, Seodaemun-gu, Seoul 120-749, South Korea*

[b] *Department of Chemical Engineering, Massachusetts Institute of Technology, 77 Massachusetts Ave., 66-325, Cambridge, MA, 02139, USA*

[*] To whom correspondence should be addressed

Tel: +82-2-2123-5757, Fax: +82-2-312-6401

E-mail: jonghak@yonsei.ac.kr

Fig. S1. (a) Plan-view SEM images of the multi-functional om-SnO_2 IF layer and (b) cross-sectional SEM image of the multi-functional om-SnO_2 IF layer coated on FTO glass.

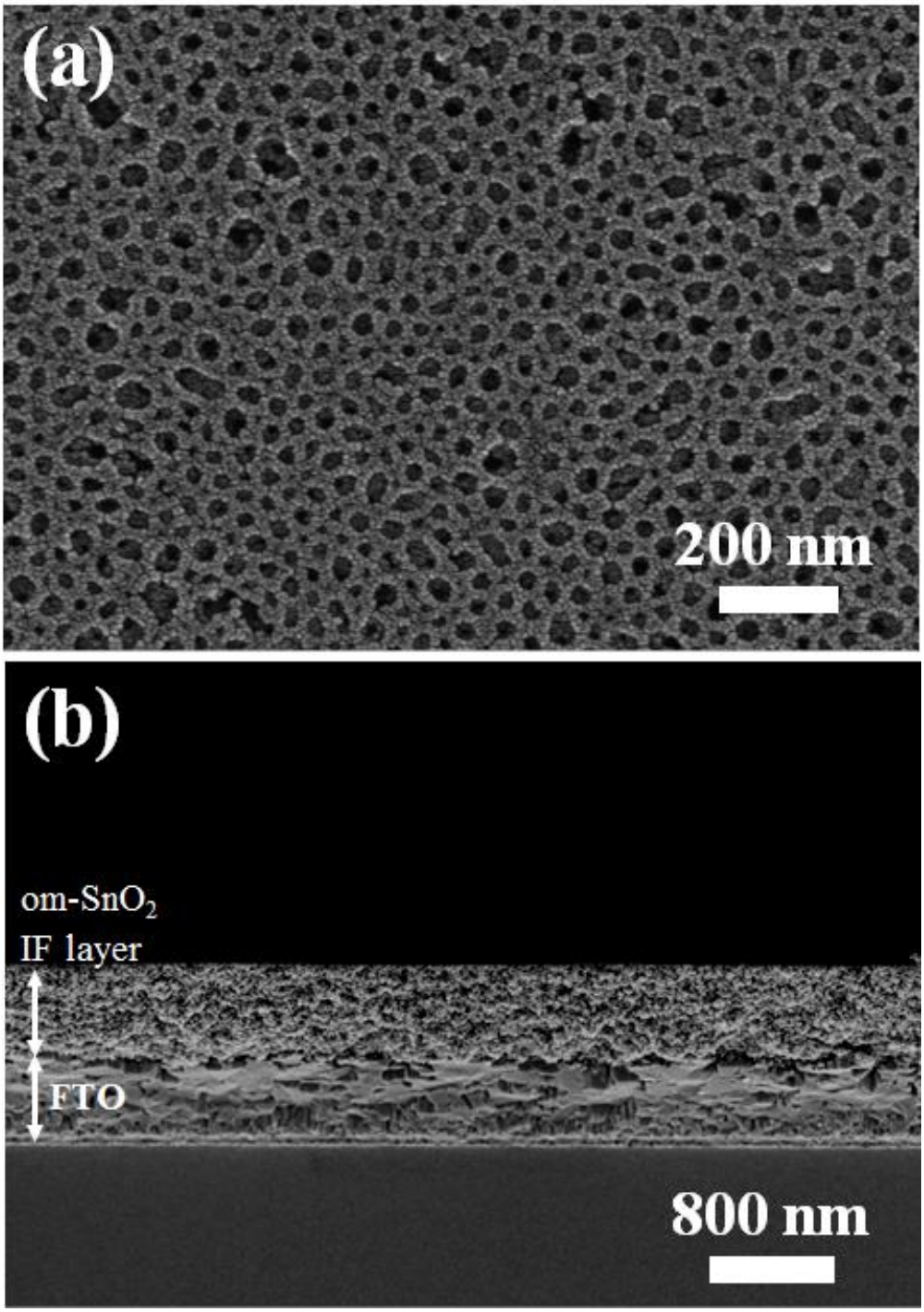

Fig. S2. Reflectance spectra of a nanocrystalline SnO_2 (NC-SnO_2) on multi-functional om-SnO_2 IF layer-coated FTO glass without N719 dye sensitizer.[a]

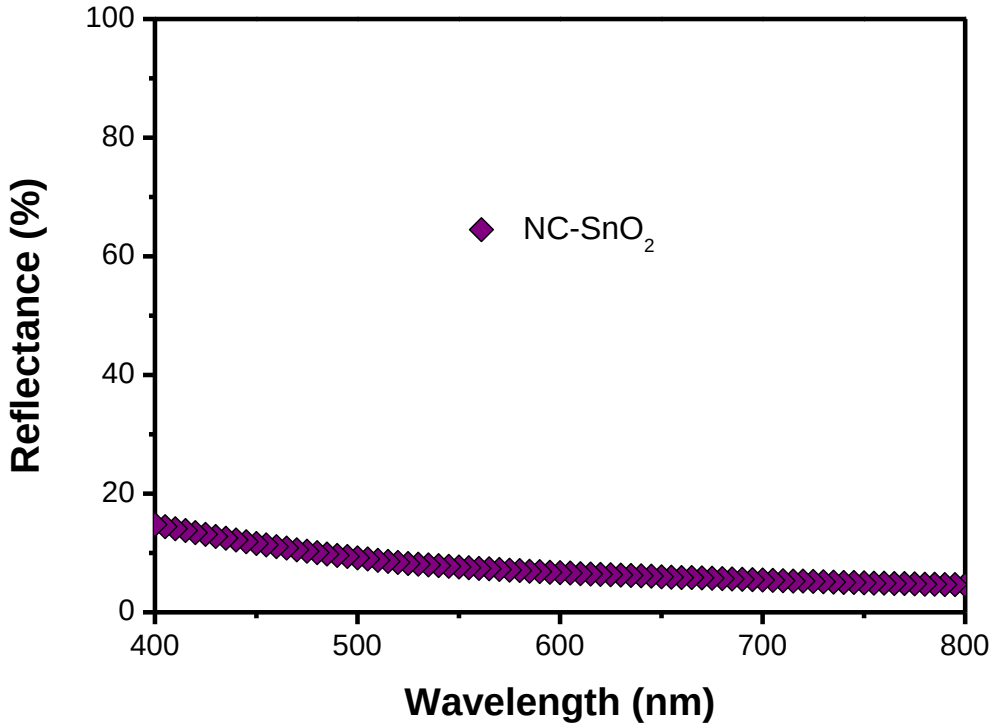

[a] commercially available nanocrystalline SnO_2 (NC-SnO_2) was purchased from Alpha-Aesar.

Fig. S3. Photocurrent density-voltage curves of DSSCs based on NP-SnO_2 spheres and HM-SnO_2 spheres on a multi-functional om-SnO_2 IF layer photoanode with liquid state electrolyte under AM 1.5G one sun light intensity.

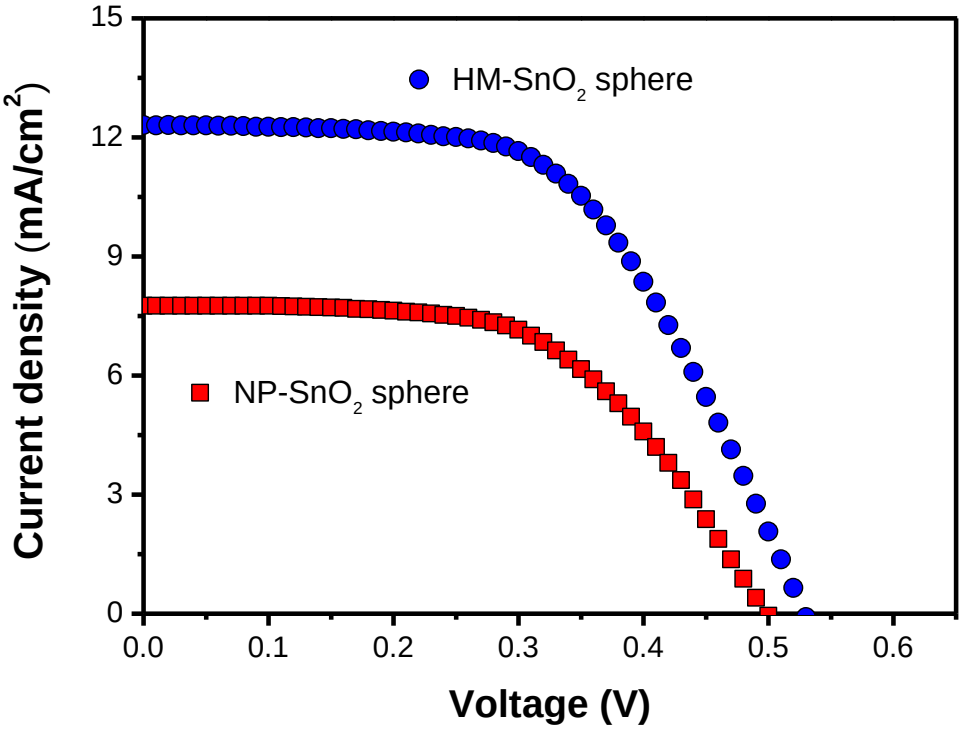

Fig. S4. Normalized efficiencies of ssDSSCs with HM-SnO_2 spheres on a multi-functional om-SnO_2 IF layer photoanode as a function of time.

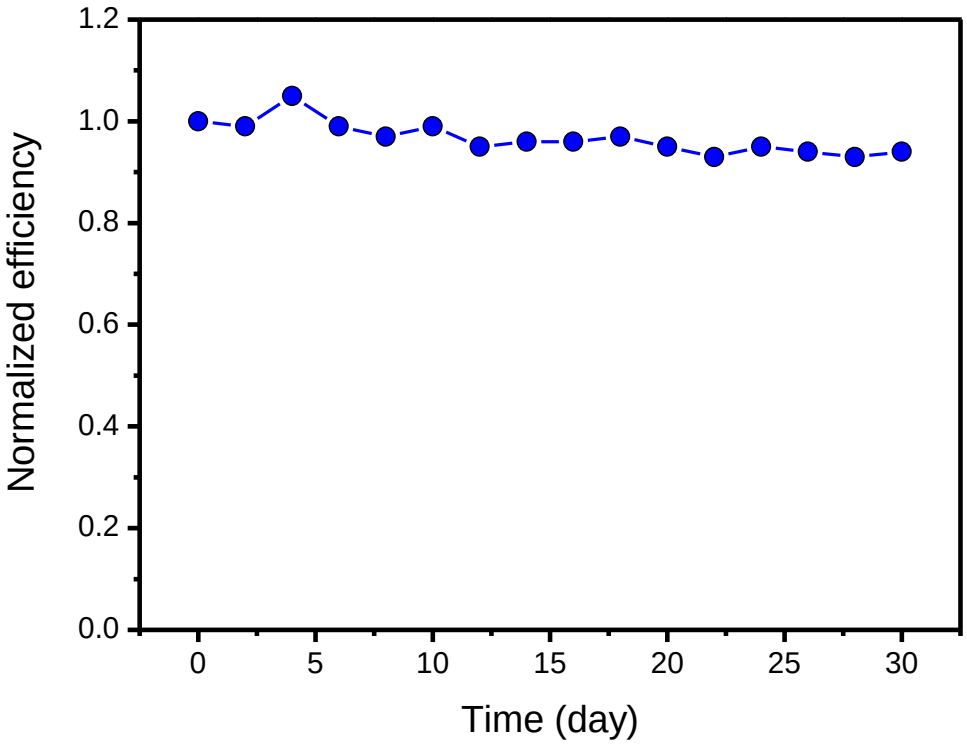

Fig. S5. Photocatalytic reactions of Degussa P25 with methyl orange under UV irradiation.

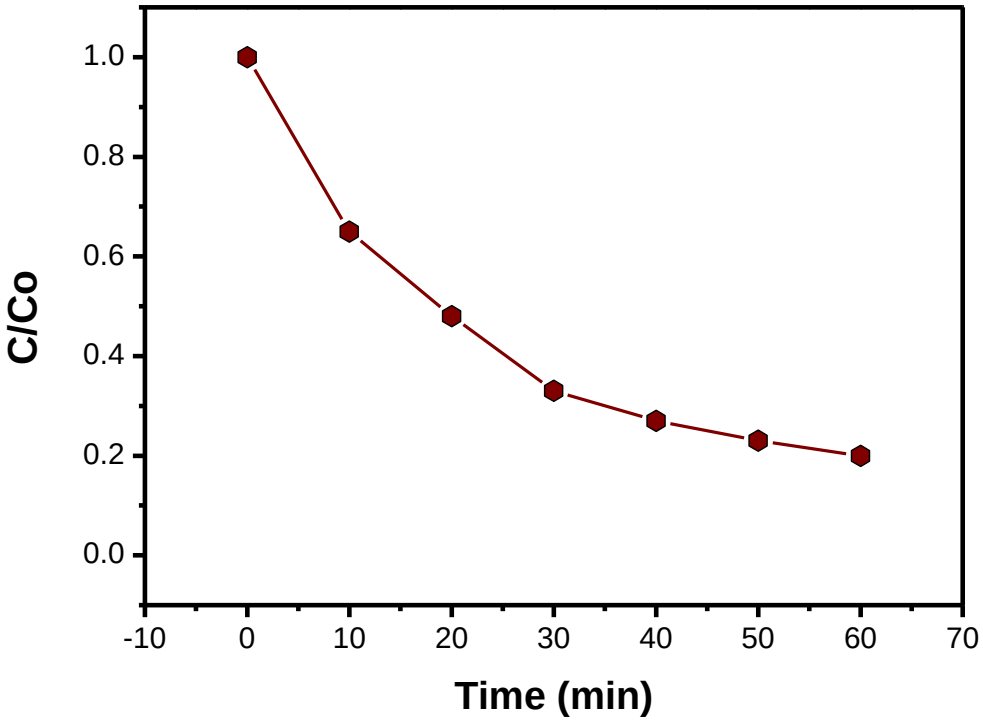

Fig. S6. Pseudo-first-order kinetic rate plots of methyl orange with NP-SnO_2 spheres and HM-SnO_2 spheres.

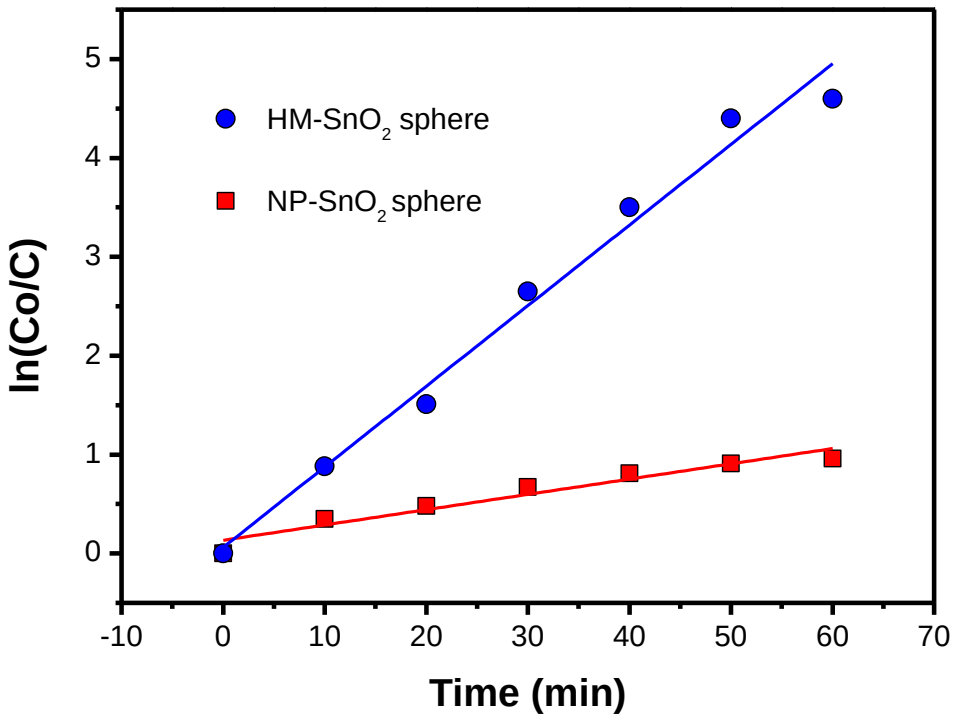

In pseudo-first-order kinetics of ln(Co/C)=*kt*, where Co/C is the normalized methyl orange concentration, *t* is the reaction time, and *k* is the rate constant.[1]

Table S1. Dye adsorption values for NP-SnO_2 spheres/om-SnO_2 IF layer and HM-SnO_2 spheres/om-SnO_2 IF layer photoanode.

Photoanode	Absorption at 515nm	Dye adsorbed ($nmol/cm^2$)	Dye adsorbed (mg/cm^2)
NP-SnO_2 spheres/om-SnO_2 IF layer	0.035	63.1	0.075
HM-SnO_2 spheres/om-SnO_2 IF layer	0.062	109.3	0.129

The N719 dye-sensitized SnO_2 photoanodes were dipped into 10mL of 0.01Maqueous ethanolic (1:1) alkaline solution of NaOH. The mixtures were stirred until complete desorption of the N719 dye. The volume of the alkali solution containing the fully desorbed dye was carefully measured by UV–visible spectroscopy at 515 nm. The adsorbed dye was calculated according to the Beer-Lambert law.[2]

Reference

1 V. Iliev, D. Tomova, L. Bilyarska, G. Tyuliev, *Journal of Molecular Catalysis A: Chemical* 2007, **263**, 32.

2 C.M. Leroy, C. Olivier, T. Toupance, M. Abbas, L. Hirsch, S. Ravaine, R. Backov, *Solid State Sciences* 2014, **28**, 81.